Chapter 5
MXenes for Energy Harvesting and Storage Applications

Rameez Ahmad Mir, Amardeep Amardeep, and Jian Liu

5.1 Introduction

Energy harvesting plays a crucial role in fabricating and utilizing new clean energy, self-powered electronic, and energy storage devices. Environmental pollution and the energy crisis are the major concerns faced by society. To address these prevailing issues, the need for new, clean, and renewable resources is increasing rapidly for sustainable energy. Hydrogen energy derived from water (a renewable source) is considered as a promising approach exhibiting a high-energy density and zero emission of toxic gases [1]. At the same time, the demand for self-powered microelectronic devices is rapidly increasing for sustainable development and smart living. For it, there is a need to develop micro-size efficient charge storage devices like new-generation batteries and supercapacitors that have attained special attention all over the globe to replace traditional bulk devices. Various materials and strategies have been developed for energy harvesting depending on their chemical and physical features. Among the developed materials, two-dimensional (2D) structures exhibiting idiosyncratic structural, morphological, and surface characteristics appeared as the potential source for energy production and storage devices. 2D materials, referring to sheet-like structures or thin films, exhibit an atomic layer thickness and high lateral dimensions [2]. MXenes, a special class of 2D transition metal carbides/nitrides (TMCs/TMNs), appeared as attractive materials for energy harvesting due to their unique physical and chemical properties. MXenes have the general formula

R. A. Mir (✉) · A. Amardeep · J. Liu
School of Engineering, Faculty of Applied Science, The University of British Columbia, 3333 University Way, Kelowna, BC V1V 1V7, Canada
e-mail: rameez.mir@ubc.ca

A. Amardeep
e-mail: amardeep.amardeep@ubc.ca

J. Liu
e-mail: jian.liu@ubc.ca

O. P. Pandey and P. Sharma (eds.), *MXenes: Emerging 2D Materials*,
https://doi.org/10.1007/978-981-97-4064-2_5

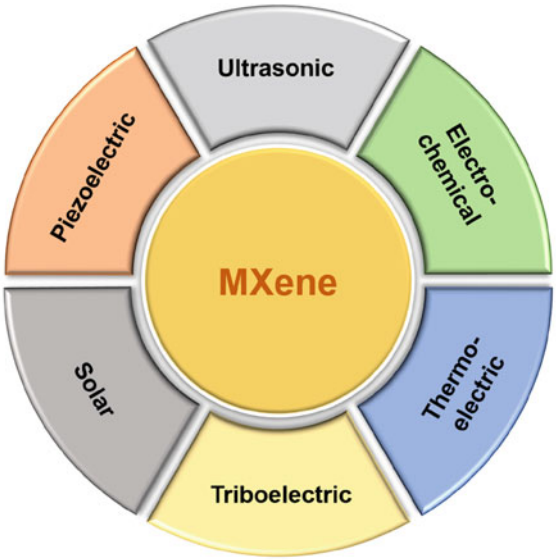

Fig. 5.1 Energy harvesting by MXene-based energy devices

$M_{n+1}X_nT_x$, where M is transition metal, X is carbon or nitrogen, and T is a functional group like fluorine, hydroxyl, or oxygen is a good source of energy harvesting and storage [3, 4]. MXene-based materials are used for harvesting different energy resources, as shown in Fig. 5.1.

Energy harvesting has a broader scope, so this chapter presents a perspective on using MXenes to harvest energy (production and storage) from different environment-friendly renewable energy sources [5]. MXenes emerged as demanding electrocatalyst materials for energy production, such as hydrogen fuel derived from water (water electrolysis) through hydrogen evolution reaction (HER)/oxygen evolution reaction (OER) and electrochemical energy storage (supercapacitors and batteries) due to their excellent electronic conductivity, large specific surface area, tuneable properties, and unique micrographical features [4, 6–8]. The typical electrochemical energy production and storage applications of MXenes are shown in Fig. 5.2.

The different characteristics and structural properties of MXenes, dependent on the synthesis methodologies, which influence energy production and storage abilities and have already been described [10]. Efforts have been made to investigate and improve the performance of 2D materials, especially MXenes, due to potentially prolonging Moore's law in energy production and storage [11]. Along with the unique chemical and physical properties of MXenes, a high population of active electrochemical sites or electrochemical active surface area (ECSA) within a small size and high mechanical stability widens their scope as electrocatalysts for hydrogen production. The essential features of MXenes, responsible for their improved charge storage performance, are high hydrophobicity and unique surface charge distribution [12]. The utilization of nanostructured MXenes gained special attention in

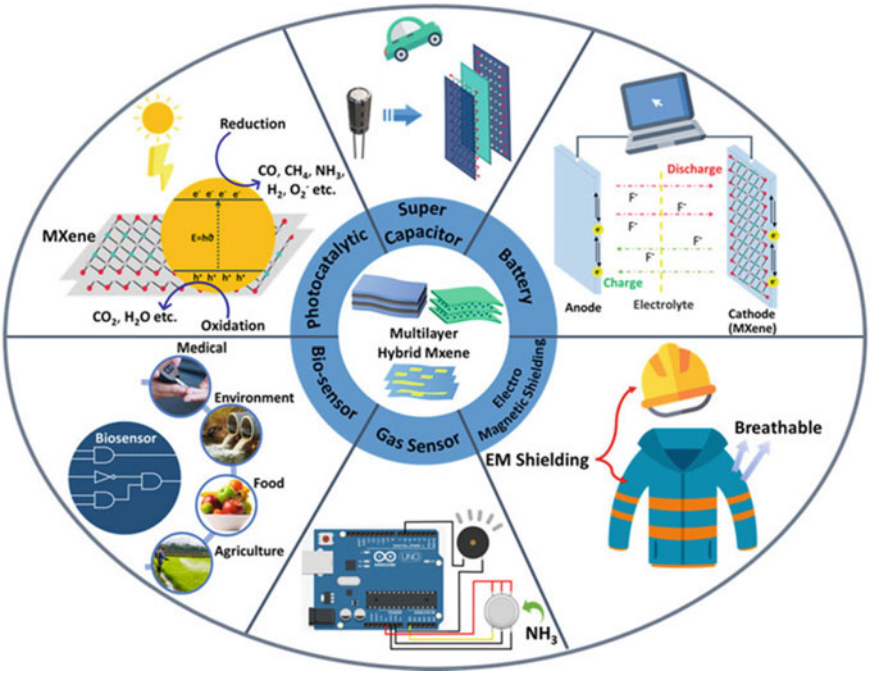

Fig. 5.2 Essential energy harvesting applications of MXenes [with permission Ref. [9] 2022 American Chemical Society]

energy production and storage due to the improvement of the surface features at the nanoscale and rapid operating mechanisms. The role of MXenes in hydrogen production, supercapacitors, and batteries are discussed as follows.

5.2 MXenes for Hydrogen Production (HER/OER)

Currently, the maximum portion of the energy is generated from traditional fossil fuels, and the reservoirs of these fossil fuels are diminishing. Moreover, the utilization of these fossil fuels generates toxic gases, which affect the environment and cause a critical issue of global warming. To address this problem, a global initiative is on the rise seeking the use of natural (renewable) and clean energy alternatives to diminishing traditional resources. Various natural energy resources, such as solar, wind, tidal, and biomass, are being explored for sustainable development. The regional or seasonal factors affect the intermittent availability of these energy sources [13]. Among the available natural resources, water-derived hydrogen (H_2) fuel exhibits different advantages, such as high purity green fuel (zero emission of toxic gases). Water electrolysis is considered as an efficient and suitable method for producing

hydrogen either through HER or OER, as shown in Fig. 5.3a. HER at the cathode (water reduction) and OER at the anode (water oxidation) in the water electrolyzer systems are kinetically sluggish and require large overpotentials for water reduction/oxidation, resulting in low energy efficiency. The electrocatalyst is vital in lowering the water-splitting potential and enhancing efficiency. The prominent role of the electrocatalyst in reducing the overpotential and energy barrier for HER and OER is shown in Fig. 5.3b–c [14].

The theoretical potential to generate hydrogen from water is 1.23 V (Fig. 5.3c). However, in practical applications, the required potential is higher than the theoretical value due to the involvement of various resistances in the water electrolyzer systems [14]. Different electrocatalyst species have been developed and tested to lower the water oxidation and reduction potentials [16, 17]. To date, platinum (Pt) or Pt/C and ruthenium oxide (RuO_2), and iridium oxide (IrO_2) exhibited potential results for efficient HER and OER, respectively. The lower abundance and high cost of noble metal electrocatalysis limit their practical/commercial implications. Different metal and non-metal electrocatalysts specie as substitutes to noble metals have been developed, such as transition metal (TM) oxides (TMOs), transition metal dichalcogenides

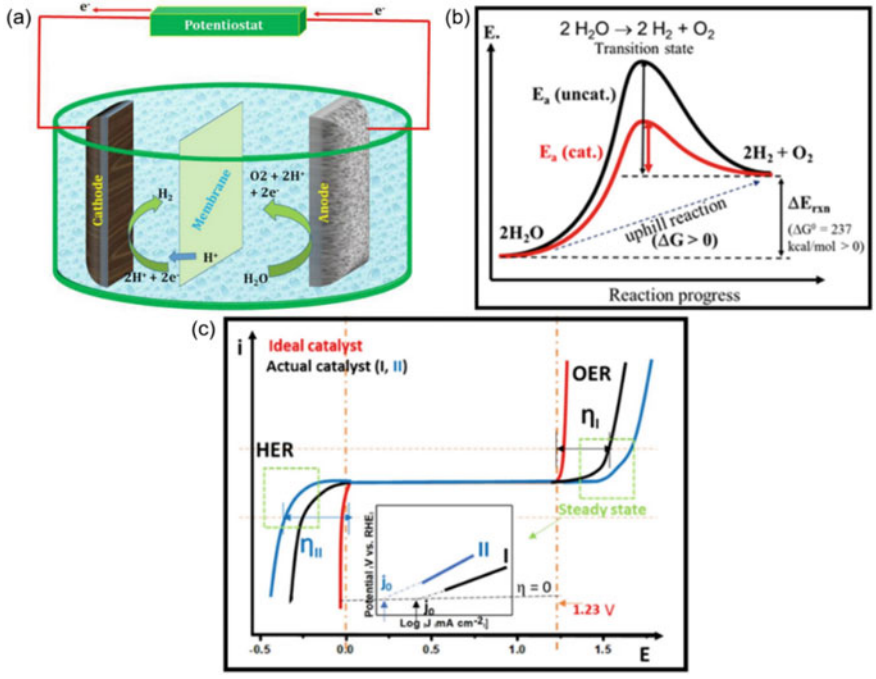

Fig. 5.3 Schematics diagram of water electrolysis, **a** HER/OER processes, [with permission Ref. [14] 2023 Elsevier] and **b–c** role of electrocatalyst in HER and OER [with permission Ref. [15] 2021 Springer]

(TMDCs), TM carbides (TMCs), TM nitrides (TMNs), non-metal supported combinations like graphene species, carbon nitride, and carbon supported electrocatalysts, etc. [14, 18–21]. With advances in 2D material electrocatalysts, especially graphene, graphene-like materials such as TMCs and TMNs showed potential to replace costly noble metal electrocatalysts due to their higher carrier mobility and intrinsic layered structure. One of the essential properties of TMCs and TMNs, which makes them attractive, is their similar electronic structure to noble metal elements like Pt and are considered as a potential candidate to replace Pt and IrO_2/RuO_2 electrocatalysts in HER and OER, respectively [22, 23]. To enhance the HER and OER activity and stability of the TMCs/TMNs, the 2D MXenes attained attention due to their exceptional intrinsic and extrinsic characteristics. The band structure of MXenes similar to Pt (due to carbon incorporation in a metal lattice), a higher number of edge sites and improved active sites due to attached functional groups on the surface, improved the water-splitting performance. Different MXene species based on TM (Ti, Mo, and V) have been developed and utilized as electrocatalyst candidates for HER and OER [24–26]. Modifying the terminal ends of MXenes enhances the HER performance by improving the conductivity and surface edge sites. For practical applications and higher efficiency, the long-term stability of the electrocatalyst is the need of time. Lim et al. [27] developed Mo_2CT_x MXene as a low cost, highly active, and stable electrocatalyst for HER. The hybrid of $Mo_2CT_X/2H\text{-}MoS_2$ MXene revealed higher stability and performance in an aqueous electrolyte. The synthesized hybrid electrocatalyst requires an overpotential of 119 and 182 mV to yield a current density of 10 and 100 mA cm^{-2}, respectively. The strong interfacial adhesion in the hybrid structure reduces the HER overpotential by tailoring the MXene sulfidation. Moreover, the $2H\text{-}MoS_2$ layer over MXene suppresses the oxidation of the MXene layers. It restricts the excessive coverage or blockade of the active interfaces that improve the charge transfer rate (high current density) without deterioration. The hybrid phase exhibits exceptionally longer durability, up to 10 days/100,000 CV cycles without degradation. The results revealed that in-situ sulfidation is a promising strategy for creating intimate interfaces among different materials and TMDCs for widening their scope in energy conversion systems. Anasori et al. [28] developed ordered double-transition metal MXene $Mo_{2+\alpha}Nb_{2-\alpha}C_3T_x$ MAX phases ($0 \leq \alpha \leq 0.3$) with different compositions as a suitable electrocatalyst for HER, as shown in Fig. 5.4.

Ordering bimetals (Fig. 5.4b–c) such as Mo (outer layer) and Nb (inner layer) affects the HER activity. The synthesized MXene phase exhibits improved HER activity (higher cathodic current) with respect to other MXene phases due to the ordering of double TMs (Fig. 5.5a). The $Mo_{2+\alpha}Nb_{2-\alpha}C_3T_x$ phase requires a lower overpotential than other MXene phases with varying Nb content, as shown in Fig. 5.5b. The said phase also outperforms the other electrocatalysts due to its lower Tafel slope of 91 mV dec^{-1} (Fig. 5.5c), indicating improved charge transfer kinetics.

The influence of Mo and Nb content on conductivity and flake size (Fig. 5.5d) revealed that the HER performance is not likely affected by the flake size, but the occupancy of Mo and Nb (metal) sites plays a key role. The HER performance hasn't yet reached the level determined by costly Pt/C electrocatalysts. The availability of the MXene precursors (transition metals and carbon) on earth determines

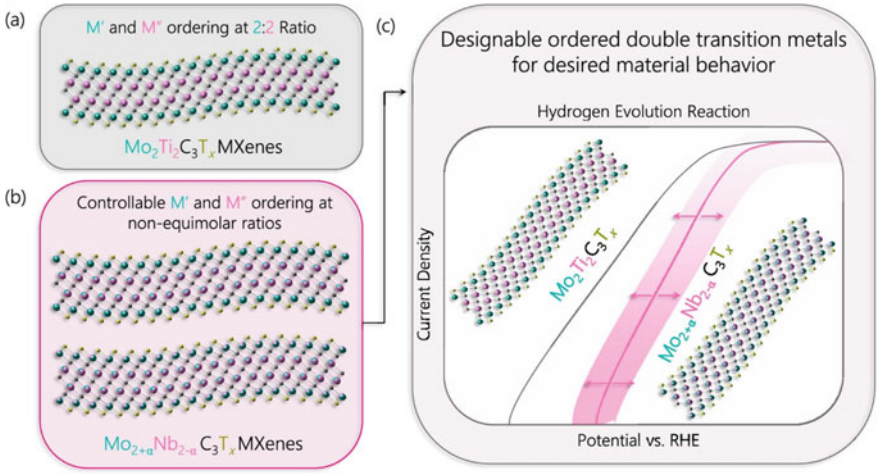

Fig. 5.4 **a** Ordering of $Mo_2Ti_2C_3T_x$ MXenes, where TMs are segregated into separate M atomic layers. **b** $Mo_{2+\alpha}Nb_{2-\alpha}C_3T_x$ MXenes allow controllable ordering in the M layers, and **c** The gained control in $Mo_{2+\alpha}Nb_{2-\alpha}C_3T_x$ MXenes, permits designable material behavior, as demonstrated in HER electrocatalytic applications [with permission Ref. [28] 2023 American Chemical Society]

the potential use of MXenes as a cost-effective electrocatalyst in water electrolyzers. Further modifications are required at both intrinsic and extrinsic levels to boost the activity and stability of MXenes compared to noble metal electrocatalysts. Along with HER in acidic electrolytes, electrocatalytic water splitting is preferred in alkaline electrolyzers. However, the need for suitable electrocatalysts is still in demand due to sluggish OER kinetics, a four-electron transfer reaction [29]. The hydrophobic nature of the MXenes allows the coverage of OH^- ions on the surface-active sites, which improves the formation of O_2, and the structural characteristics enhance the ability of O_2 evolution [30]. Yan et al. [31] synthesized nine atomic layered reactive surface modified (RSM) $V_4C_3T_x$ MXene. The surface modifications with the different amorphous metal hydroxides (Ni, Fe, and V hydroxides) formed during the in-situ process improve the inner skeleton's stability ($V_4C_3T_x$) without disrupting it. The synthesized nanohybrids exhibited higher OER stability for more than 70 h. The exceptional HER/OER activity and stability of the MXene nanohybrids present a significant step forward in exploring the MXenes as non-noble electrocatalysts for water splitting. Various categories of MXenes have been developed and explored as suitable electrocatalysts for HER and OER. The corresponding HER/OER performance of these MXenes is given in Table 5.1, exhibiting better electrocatalytic properties than other metal/non-metal electrocatalysts. However, the relatively higher cost due to typical synthesis procedures and a slightly higher overpotential than Pt/C still restricts their potential applications in commercial systems. Efforts are being made to synthesize them with easy and manageable strategies to improve their activity higher than Pt/C. The further exploration and design modification of the MXene

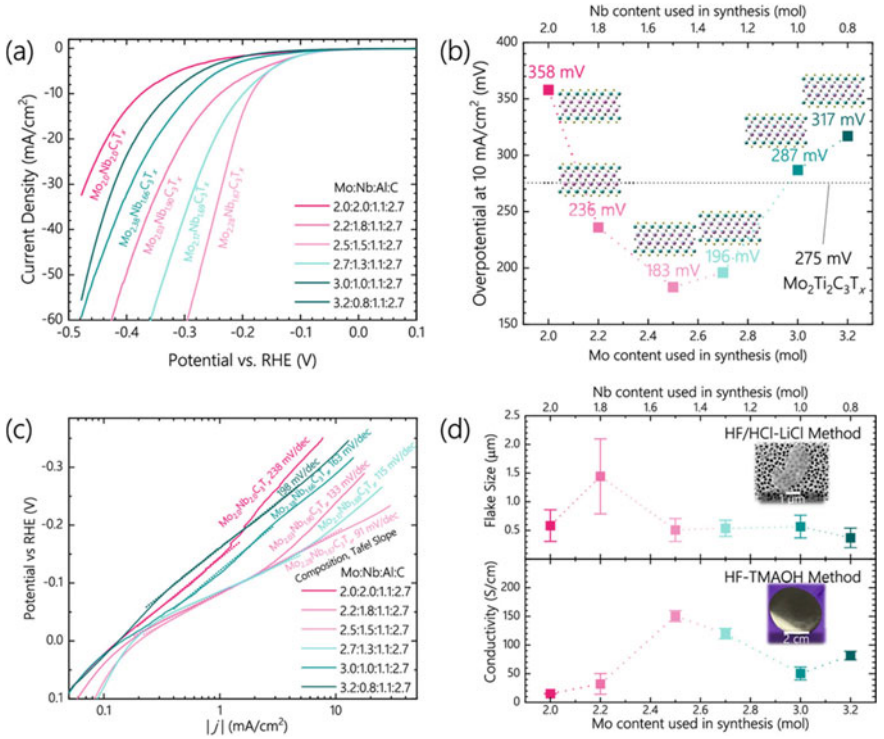

Fig. 5.5 HER activity of HF/HCl-LiCl-produced $Mo_{2+\alpha}Nb_{2-\alpha}C_3T_x$ MXenes. **a** I–V plots of $Mo_{2+\alpha}Nb_{2-\alpha}C_3T_x$ MXenes (Mo:Nb:Al:C composition in legend, actual Rietveld-derived composition next to data) used to derive overpotentials at 10 mA/cm^2 and Tafel slopes are shown in **b** and **c**, respectively. **d** Conductivity measurements of HF-TMAOH-synthesized $Mo_{2+\alpha}Nb_{2-\alpha}C_3T_x$ MXenes compared to flake sizes of HF/HCl-LiCl-synthesized $Mo_{2+\alpha}Nb_{2-\alpha}C_3T_x$ MXenes [with permission Ref. [28] 2023 American Chemical Society]

family contributes to the energy production application. Along with energy production applications, the MXenes also revealed exceptional energy storage performance in both supercapacitors as well in batteries, as discussed below.

5.3 MXenes for Supercapacitors

Supercapacitors, also known as ultracapacitors or electrochemical supercapacitors (ESs), are special systems for energy storage due to their rapid charging characteristics and high storage ability compared to conventional capacitors [10, 56, 57]. The fast adsorption and desorption of electrolyte ions on the electrode surface exhibited a higher efficiency than conventional capacitors. Figure 5.6 shows the basic design of the supercapacitors.

Table 5.1 Performance of different MXenes in HER and OER

Sample	Reaction	Tafel slope (mV dec^{-1})	Overpotential at 10 mA cm^{-2} (mV)	Electrolyte	References
MXene electrocatalysts for HER					
Mo_2CT_x	HER	74.0	189	0.5 mol/L H_2SO_4	[32]
$Ti_3C_2T_x$	HER	128.0	538	0.5 mol/L H_2SO_4	[33]
F-terminated Ti_2CT_x	HER	100.0	170	0.5 mol/L H_2SO_4	[34]
O-terminated $Ti_3C_2T_x$	HER	60.7	190	0.5 mol/L H_2SO_4	[35]
$V_4C_3T_x$	HER	168.0	200	0.5 mol/L H_2SO_4	[36]
N-Ti_2CT_x	HER	67.0	215	0.5 mol/L H_2SO_4	[37]
$Ti_3C_2T_x$ nanofibers	HER	97.0	169	0.5 mol/L H_2SO_4	[38]
$Ni_{0.9}Co_{0.1}$@Nb-$Ti_3C_2T_x$	HER	116.0	43.4	1.0 mol/L KOH	[39]
Pt/$Ti_3C_2T_x$-550	HER	32.3	32.7	0.1 mol/L $HClO_4$	[40]
TBA-$Ti_3C_2T_x$-Pt-20	HER	85.0	70	0.5 mol/L H_2SO_4	[41]
Co^{3+}-Cr_2CT_x	HER	112.0	404	1.0 mol/L KOH	[42]
Co^{3+}-V_2CT_x	HER	98.1	460	1.0 mol/L KOH	
Co^{3+}-Ti_2CT_x	HER	103.0	458	1.0 mol/L KOH	
Co-MoS_2@Mo_2CT_x	HER	82.0	112	1.0 mol/L KOH	[43]
PtNPs/$Ti_3C_2T_x$	HER	59.54	226	0.5 mol/L H_2SO_4	[44]
MoS_2-Ti_3C_2	HER	40.0	110	0.5 mol/L H_2SO_4	[45]
PtO_aPdO_bNPs@$Ti_3C_2T_x$	HER	70.0	57	0.5 mol/L H_2SO_4	[46]
MoS_2/Ti_3C_2 MXene@C	HER	45.0	135	0.5 mol/L H_2SO_4	[47]
MoS_2/$Ti_3C_2T_x$ nanoroll	HER	70.0	168	0.5 mol/L H_2SO_4	[48]

(continued)

Table 5.1 (continued)

Sample	Reaction	Tafel slope (mV dec^{-1})	Overpotential at 10 mA cm^{-2} (mV)	Electrolyte	References
CoP@3D $Ti_3C_2T_x$	HER	58.0	168	1.0 mol/L KOH	[49]
MXene electrocatalysts for OER					
FeNi-LDH/$Ti_3C_2T_x$	OER	43.0	298	1.0 mol/L KOH	[50]
$Ti_3C_2T_x$-CoBDC	OER	48.2	410	0.1 mol/L KOH	[51]
g-C_3N_4/$Ti_3C_2T_x$ film	OER	74.6	420	0.1 mol/L KOH	[52]
Co-Bi/$Ti_3C_2T_x$	OER	53.0	250	1.0 mol/L KOH	[25]
S-$NiFe_2O_4$@Ti_3C_2@NF	OER	46.8	270	1.0 mol/L KOH	[53]
NiCoS/$Ti_3C_2T_x$	OER	58.2	365	1.0 mol/L KOH	[54]
Co^{3+}-Ti_2CT_x	OER	63.2	420	1.0 mol/L KOH	[42]
PtO_aPdO_bNPs@$Ti_3C_2T_x$	OER	78.0	310	0.1 mol/L KOH	[46]
$Ni_{0.7}Fe_{0.3}PS_3$@ $Ti_3C_2T_x$	OER	36.5	282	1.0 mol/L KOH	[47]
Co/N-CNTs@$Ti_3C_2T_x$	OER	79.1	411	0.1 mol/L KOH	[55]
CoP@3D $Ti_3C_2T_x$	OER	51.0	280	1.0 mol/L KOH	[49]

The essential features of supercapacitors are that they exhibit high power density and long-term cyclic stability than traditional capacitors and batteries. Progress has been made to improve the performance, especially the energy density of the ESs, by developing suitable and stable electrode materials that enable the electron transfer and ion diffusion process to occur rapidly and reversibly. On account of the energy storage mechanism, ESs have been classified as electrochemical or electrical double-layer capacitors (EDLCs), pseudocapacitors, and newly introduced hybrid supercapacitors that store and release energy based on non-Faradic and Faradic interactions at the electrode–electrolyte interface, respectively [59–61]. In the case of EDLCs, a double-layer is formed between the ions in the electrolyte and the attracted electrons on the electrode surface. In contrast, the charge is stored in pseudocapacitors by the rapid, reversible Faradic reactions on the electrode surface. The adsorption of electrolyte ions is very fast in EDLCs and the Faradic charge transfer during the pseudocapacitive

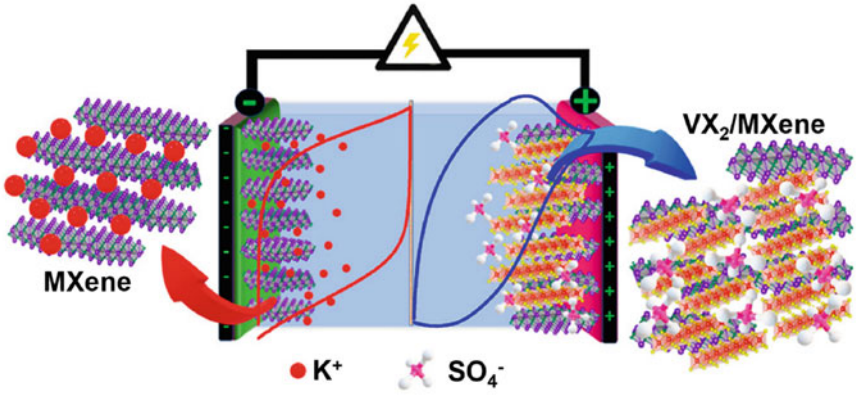

Fig. 5.6 Schematic diagram of electrochemical MXene-based supercapacitor [with permission ref. [58] 2021 American Chemical Society]

process is sluggish but stores more energy than EDLCs. The major drawback of the ESs based on aqueous electrolytes is the small voltage window restricted by the thermodynamic stability of water [62]. The prevailing issues with charge storage devices are the lower energy and power density exhibited by supercapacitors and batteries. To overcome these drawbacks, hybrid supercapacitors (HSCs) combine the energy storage mechanism revealed by the capacitors and batteries. HSCs consist of different electrode materials, a battery or pseudocapacitors type anode and a capacitor type cathode to improve energy and power density, respectively. Carbon-based electrodes are common in EDLCs, pseudocapacitors, and HSCs. Carbon materials exhibiting higher surface area act as electrodes for EDLCs revealing high power density, but the energy density is still not comparable to batteries. Efforts have been made to improve the energy density of ESs. The pseudocapacitors exhibited higher charge transfer kinetics based on the redox reaction mechanism and enhanced the energy density of the ESs. Advanced electrode materials are being searched and developed with a high specific area, high conductivity, and rich redox sites that are highly desired for developing high-performance supercapacitors [10]. To date, different categories of electrodes have been developed, like carbon species, CNTs, mesoporous carbon, carbon shells, transition metal oxides (TMOs), 2D materials like graphene species, transition metal dichalcogenides (TMDCs), transition metal carbides (TMCs) and transition metal nitrides (TMNs). The electrochemical charge storage ability of the well-known 2D material (graphene) is finite due to the absence of redox reactions and the main portion of capacitance arises due to EDLC mechanism. TMOs, especially like MnO_2 and RuO_2 being pseudocapacitive materials, exhibited higher capacitance and energy densities, but the cyclic stability is still lower than the carbon electrodes. Among the developed materials, the 2D TMCs/TMDs, especially the MXenes, have attained special attention as electrode materials for ESs due to a particular layered

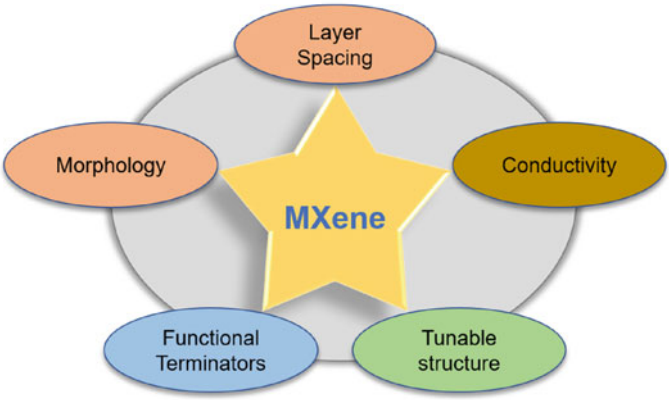

Fig. 5.7 Required features for MXene-based electrodes for energy storage

structure, faster electrolyte ion transport kinetics, and higher number of surface-active redox sites [10]. Figure 5.7 shows the main characteristics of MXenes that enhance the charge storage performance.

The distance between the layers of the MXene electrode forms the channels to improve the ion transport favorable for EDLCs. However, the outermost TMO or the functional groups on the surface layer provides redox-rich sites necessary for making pseudocapacitive energy storage possible. The inner layer of TMCs in MXenes exhibited excellent electron conductivity [57]. Various strategies have been followed to improve the charge storage ability of MXenes, such as redesigning electrodes, regulating surface functional groups, and controllable synthesis of the MXene phase [63]. Moreover, the typical synthesis procedure of the MXenes still restricts their potential applications in supercapacitor technology compared to carbon species and other metal compounds. Different MXene species have been suggested based on transition metals, but only a few have been practically synthesized [63–66]. Due to the complex chemical composition and structure, the electrolyte ion interaction of MXenes with different electrolytes (a combination of organic and aqueous electrolytes) has not been explored yet. Among all MXenes, Ti_3C_2 MXene is mostly studied due to its higher stability and ease of fabrication [67]. Most of the studies revealed that the supercapacitor performance of MXenes is highly dependent on the layered structure and the functional groups on the surface [63]. For improved energy storage in MXene-based supercapacitors, the O-terminated groups provide more electrochemical reaction sites than the –OH and –F groups [68]. Xie et al. [69] confirmed that the Li-ion storage ability of 2D MXenes depends on the surface functional groups. The –OH groups are deliberately removed through heat treatment or electrochemical reactions during the initial cycling (lithiation cycle). The lithiated oxygen-terminated surfaces of MXenes are capable of absorbing more Li-ions and provide a way to increase their capacity. The corresponding effects were observed in the delaminated MXenes, through XAS and were also revealed by the DFT studies.

The capacitance of the MXenes is mainly affected by the surface functional group that influences the conductivity and hydrophilicity. The development of the surface functional groups during the etching of the MAX phase brings hydrophilicity and affects the electronegativity of the MXene surfaces [70]. The electrolyte ion interaction with MXene affects its structural features and performance. Lukatskaya et al. [57] observed a downshift in the XRD pattern of Ti_3C_2Tx, which can be attributed to an increase in the lattice parameter (c-axis of $Ti_3C_2T_x$) in the KOH electrolyte solution. Similar results were observed in other electrolyte solutions due to cation intercalation [71]. Gogotsi et al. [72] synthesized 13-μm thick $Ti_3C_2T_x$ MXene-based electrochemical capacitors and achieved a gravimetric capacitance of 310 Fg^{-1} in 3 M H_2SO_4 solution. The highly ion-accessible MXene electrodes exhibited higher capacitance than graphene and other commercial capacitors [73–77]. Modifying the structural features of the MXene electrodes enhances the accessibility to the redox-active sites. Mesoporous $Ti_3C_2T_x$ MXene revealed a capacitance of 210 F g^{-1} even at 10 mV s^{-1}. The MXenes can deliver a ~1500 F cm^{-3} capacitance higher than state-of-the-art supercapacitor electrodes [73]. Agnese et al. [78] also studied the influence of surface modifications on the supercapacitor performance of Ti_3C_2 MXene in an H_2SO_4 solution. The two-way chemically surface modification of the Ti_3C_2 MXene is given in Fig. 5.8. The resultant product d-Ti_3C_2 (Fig. 5.8b) is due to the delamination of layers and the functional group containing Ti_3C_2 MXene (Fig. 5.8c–d) resulting from the K^+ intercalation mechanism.

The enhancement of capacitance performance in the case of MXenes revealed by the electrochemical testing was attributed to the higher number of oxygen-containing

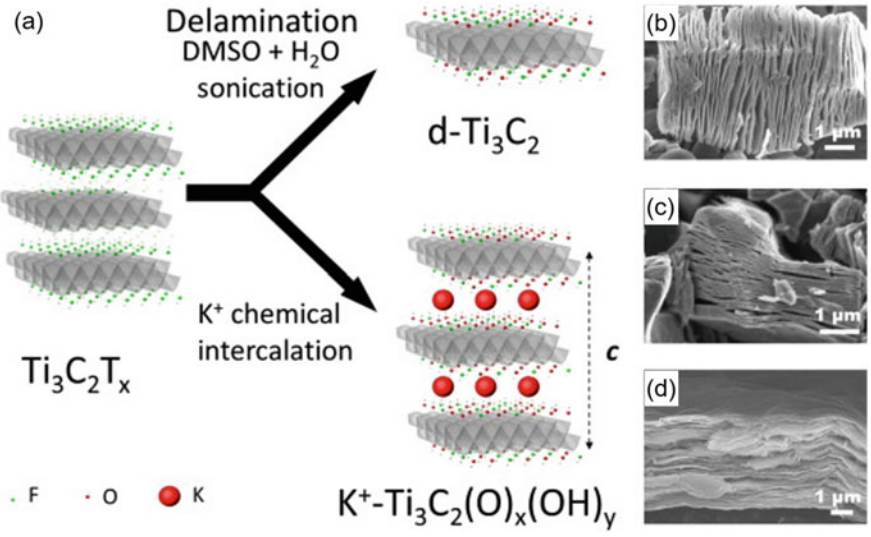

Fig. 5.8 **a** Schematic representation of the modifications of $Ti_3C_2T_x$ MXene, scanning electron microscope (SEM) images of **b** $Ti_3C_2T_x$, **c** KOH-Ti_3C_2, and **d** d-Ti_3C_2 [with permission [78] 2014 Elsevier]

functional groups. The CV plots of the synthesized material tested at 10 mV s^{-1} are shown in Fig. 5.9a. The concentrated electrolyte solution (1 M H_2SO_4 electrolyte) does not affect the lattice parameters of MXene due to the smaller size of H^+ ions compared to K^+ ions. The delaminated d-Ti_3C_2 exhibited a higher capacitance of 520 F cm^{-3} due to its thin electrode size and better charge transfer kinetics. However, the d-Ti_3C_2 MXene shows more dependency on the scan rate (Fig. 5.9b) due to the alignment of flakes parallel to the current collector.

The functional group attached to $Ti_3C_2T_x$, responsible for redox reaction (pseudocapacitive) in acidic electrolytes, was also confirmed by broad peaks in the CV curves. The transition metal (Ti in this case) in MXene can change its oxidation states from 3^+ to 4^+ due to surface redox reactions. A long-term stability test (GCD test) performed for MXenes (d-Ti_3C_2 and KOH-Ti_3C_2) shows no degradation even after 10,000 cycles (Fig. 5.9c–d). The results revealed that the surface modification of 2D MXenes is essential for improving the energy storage performance of MXene-based ESs. Zhou et al. [65] applied the DFT criteria to explore, design, and assemble the Mo_2CT_x MXenes for supercapacitors. The supercapacitor performance of the Mo_2CT_x MXene was investigated in various electrolytes such as 1 M H_2SO_4, KOH, and $MgSO_4$. The adsorption of hydrogen (H), potassium (K), and magnesium (Mg)

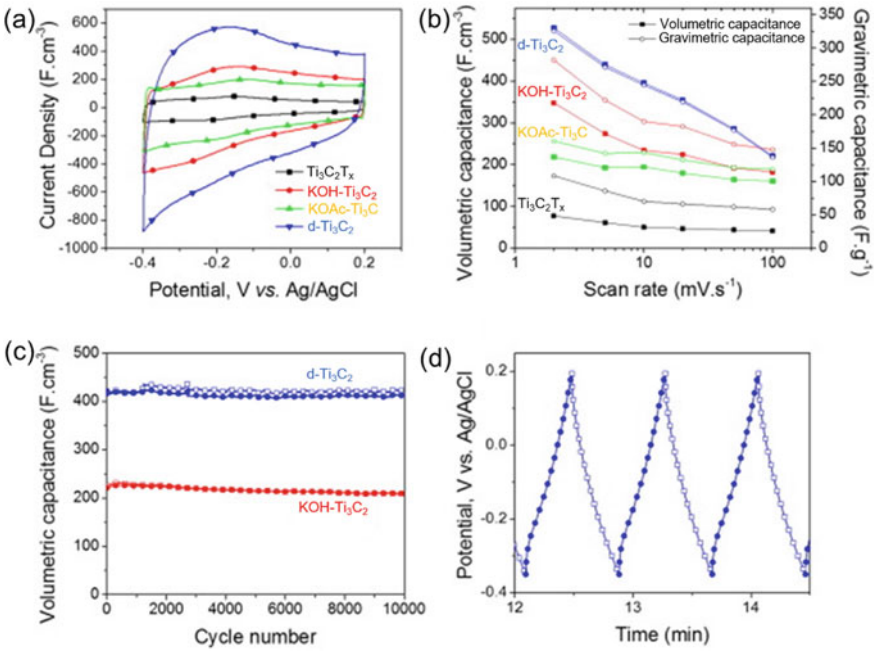

Fig. 5.9 Electrochemical activity of Ti_3C_2 MXene **a** CV profiles at 10 mV s^{-1}. **b** Summary of rate performances. **c** Charge and discharge volumetric capacitance versus cycle number of KOH–Ti_3C_2 and d-Ti_3C_2 electrodes from galvanostatic cycling at 5 A g^{-1}. **d** Galvanostatic charge–discharge profile of d-Ti_3C_2 [with permission Ref. [78] 2014 Elsevier]

on the surface of Mo_2CT_x MXene has been explored. The specific capacitance (70.14 Fg^{-1}) obtained in 1 M H_2SO_4 was more than that of KOH (11.27 Fg^{-1}) and $MgSO_4$ (18.97 Fg^{-1}). The Mo_2CT_x MXene shows a high retention rate of 89.9% (KOH), 96% ($MgSO_4$), and 98% (H_2SO_4) over 5000 cycles. After that, different MXene materials have been developed as supercapacitors based on the transition metal, electrode type, and electrolyte [73, 79]. Along with pristine MXenes, the nanocomposite of the MXenes has gained research attention as supercapacitor candidates due to the improvement in the surface properties necessary for enhancing the storage performance [79]. Luo et al. [64] explored that the tailoring of the interlayer spacing was controlled in accordance with the intercalated agent. The morphological features of the Ti_3C_2 MXene before and after the pillaring process are shown in Fig. 5.10.

The SEM micrograph of CTAB@Ti_3C_2 (Fig. 5.10a) showed the presence of some irregular particles on the Ti_3C_2 matrix, particularly the anchored CTAB. Almost no particles were observed in the Sn(IV)@Ti_3C_2 composites synthesized without the CTAB prepillaring process (Fig. 5.10b). No clear particles can be detected in the Sn(IV) nano complex assisted by CTAB prepillaring process (Fig. 5.10c−d). The TEM image of CTAB−Sn(IV)@Ti_3C_2 (Fig. 5.10e−f) shows that the Sn(IV) nanocomplexes (dot-shaped) are uniformly distributed in the CTAB@Ti_3C_2 matrix. The particle size was reduced to 2–5 nm (Fig. 5.10f) due CTAB effect, acting as the surfactant and the prepillaring agent [64, 80]. Figure 5.10g shows a clear layered structure of the MXene complex, along with the uniform distribution of constituents as observed in the mapping pattern (Fig. 5.10h−i). The remarkable energy storage performance of the developed MXene complex (CTAB−Sn(IV)@Ti_3C_2) was tested as an anode in the hybrid capacitor with activated carbon (AC) as a cathode, as shown in Fig. 5.11a.

The CV (Fig. 5.11b) plots performed at different scan rates in a wide voltage window of 1.0–4.0 V show no electrolyte decomposition. The deflection from the regular rectangular CV curve attributes to the redox reactions on the terminated surface functional groups. The fabricated hybrid capacitor revealed an energy density of 239.50 Wh kg^{-1} due to the pillaring effect. The results revealed that incorporation of the CTAB−Sn(IV)@Ti_3C_2 MXene anode with commercial AC cathode showed a better rate capability necessary for higher energy and power density supercapacitors (Fig. 5.11c). The capacitance retention is outstanding till 4000 cycles with negligible loss as shown in Fig. 5.11d. Moreover, along with the superior capacitance performance of MXenes, the other advantages such as atomic layer thickness, exceptional hydrophilic properties, micro/nanoscale dimensions, and special mechanical characteristics enable them (MXenes) to be converted into flexible electrodes. The high conductivity of MXenes attributes to higher power density than conventional semiconductor metal oxides and also provides a possible way to fulfill the need for rapid charging materials. This led to the development of semiconductor-type MXene-based supercapacitors. Qin et al. [81] developed semitransparent flexible photovoltaic supercapacitor (PSC) and transparent MXene supercapacitors by incorporating a flexible organic photovoltaic (OPV) with $Ti_3C_2T_x$ and bare $Ti_3C_2T_x$ MXene as the electrodes, respectively. The synthesis, morphological features, and size of the developed flakes are shown in Fig. 5.12. MXene integration with a flexible

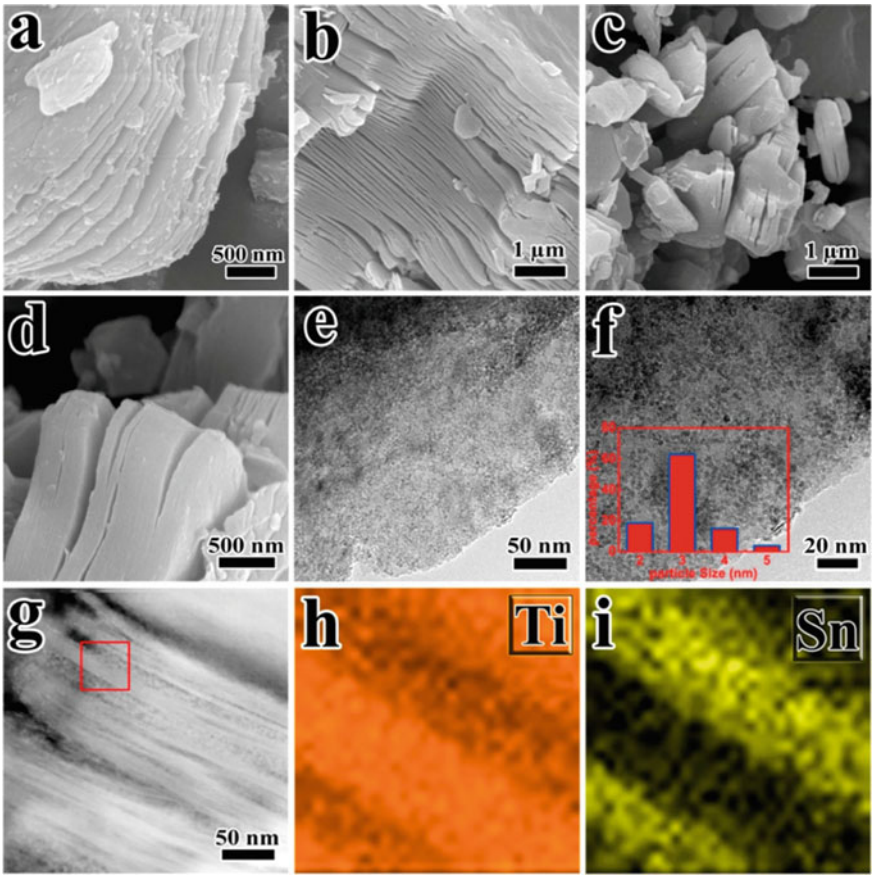

Fig. 5.10 **a** SEM image of CTAB@Ti_3C_2. **b** SEM image of Sn(IV)@Ti_3C_2 without cetyltrimethylammonium bromide (CTAB) prepillaring process. **c–f** SEM and TEM images of CTAB–Sn(IV)@Ti_3C_2. Inset in (**f**): lateral size distribution of the anchored Sn(IV) nano complex. **g–i** STEM image of CTAB–Sn(IV)@Ti_3C_2 and corresponding elemental mapping of Ti and Sn [with permission Ref. [64] 2017 American Chemical Society]

OPV photoelectrode as PSC exhibited an enhanced power conversion efficiency of 13.6%, higher than commercial indium tin oxide (ITO).

The transparent MXene-based supercapacitor exhibited a high volumetric capacitance of 502 F cm^{-3} with improved stability up to 10,000 cycles. The supercapacitor performance of the developed MXene at varying scan rates and applied currents is shown in Fig. 5.13. The cyclic voltammetry (Fig. 5.13b) plots show the retention of a nearly rectangular shape even at a higher scan rate (500 mV s^{-1}), which revealed the excellent reversible capacitive behavior of the electrode material. The results also revealed the potential applicability of the developed material as efficient electrodes for energy storage devices even at higher scan rates (>10 mV s^{-1}). The symmetric shape of the GCD curve (Fig. 5.13c) revealed that the charge/discharge process agrees

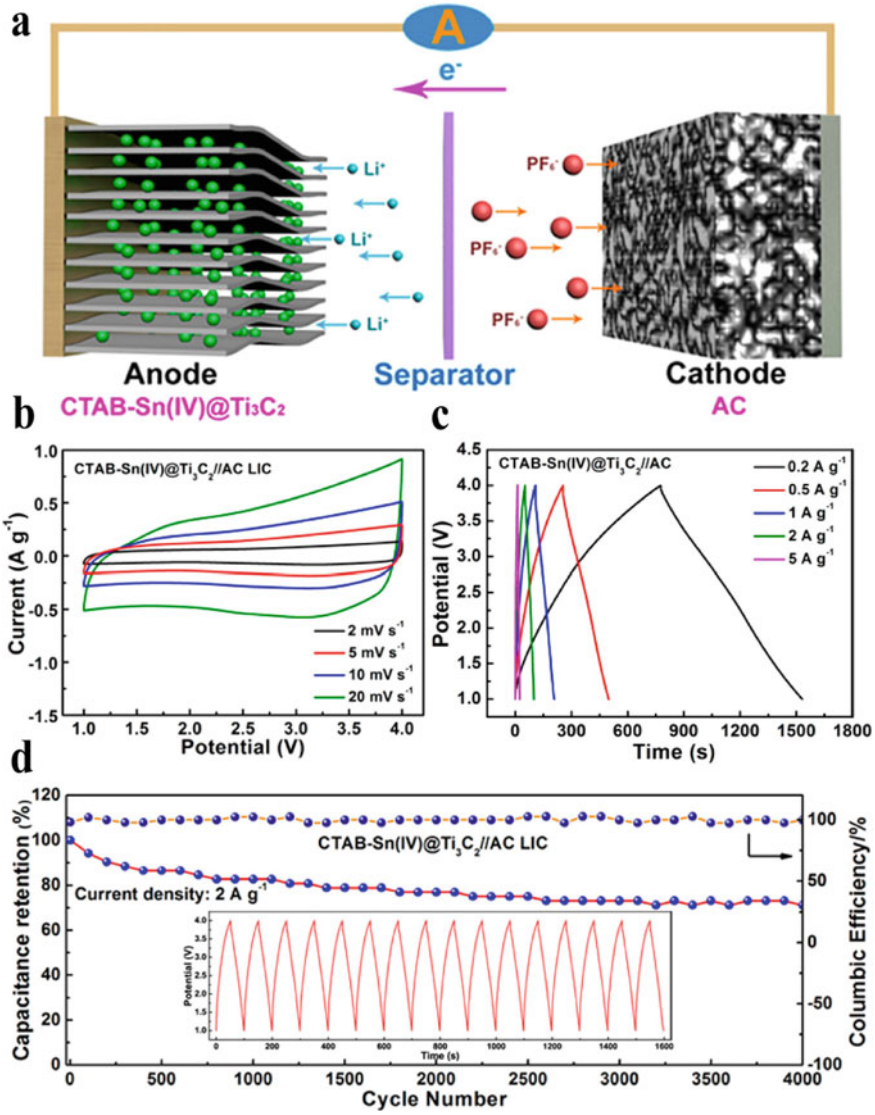

Fig. 5.11 **a** The charging process of CTAB–Sn(IV)@Ti_3C_2//AC lithium ion capacitor (LIC). **b** CV curves of CTAB–Sn(IV)@Ti_3C_2//AC LIC at different scan rates. **c** Typical charge–discharge curves of CTAB–Sn(IV)@Ti_3C_2//AC LIC at different current densities. **d** Long-term cycling performance of LIC at 2 A g^{-1}. Inset in (**d**): charge–discharge curves at 2 A g^{-1} [with permission Ref. [64] 2017 American Chemical Society]

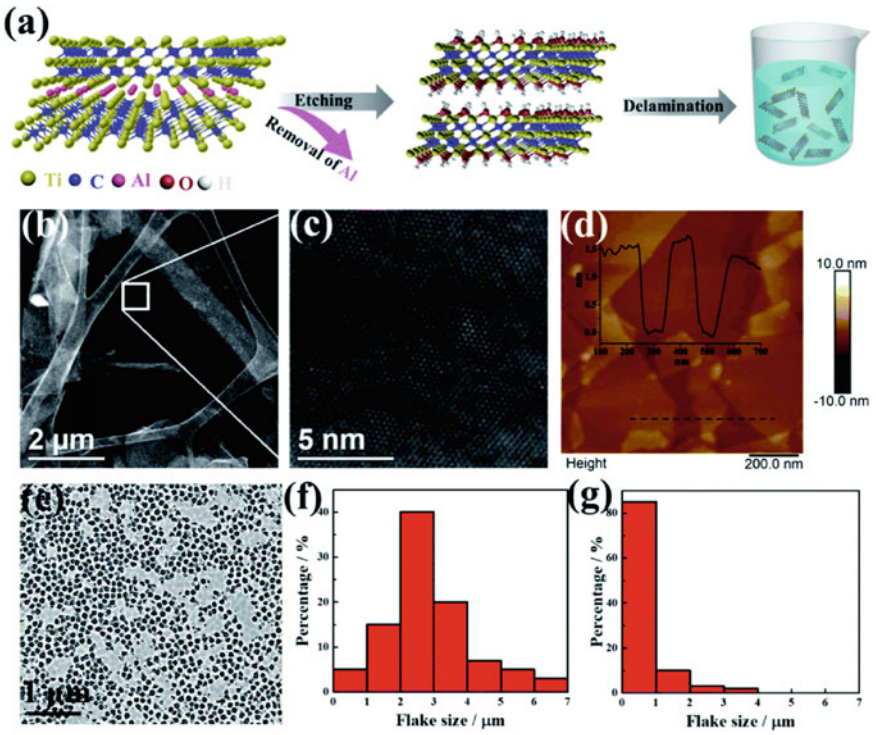

Fig. 5.12 Synthesis of the $Ti_3C_2T_x$ MXene colloidal solution. **a** preparation of MXene from the Ti_3AlC_2 precursor using the minimally intensive layer delamination (MILD) method. **b** Low-magnification and **c** high-magnification STEM images of single $Ti_3C_2T_x$ sheets dispersed onto a lacy carbon grid. **d** AFM image of a $Ti_3C_2T_x$ single layer. **e** Top view SEM image of small-sized $Ti_3C_2T_x$. The $Ti_3C_2T_x$ flake size distributions **f** before and **g** after sonication [with permission Ref. [81] 2017 (open access) Royal Society of Chemistry (RSC)]

with the CV results. The corresponding capacitance values dependent on the applied current and scan rate are given in Fig. 5.13d.

The stability of the MXene supercapacitors was analyzed by performing GCD measurements till 10,000 cycles, and the device shows a retention of 95% as that of initial capacitance. The long-term durability (Fig. 5.13e) of the fabricated supercapacitor is attributed to the non-aqueous organic solid ionogel electrolyte. This type of electrolyte overcomes the leakage issues faced in aqueous electrolytes. In addition, the MXenes can form a flexible supercapacitor, as shown in Fig. 5.13f. The obtained features like high-capacitance, long-term stability, and flexibility as different bending angles show the promising applications of $Ti_3C_2T_x$ Mxene as commercial supercapacitors. The developed PSC exhibited a high transmittance of over 33.5% and an exceptional storage capacity of 88%. This strategy widens the scope of developing the MXene-based, highly active, and stable flexible PSCs essential for printable electronics for future technologies.

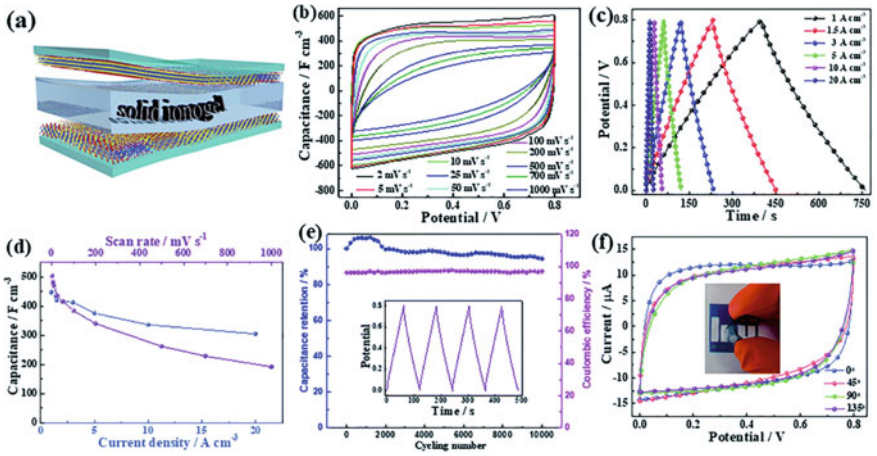

Fig. 5.13 Electrochemical performances of transparent, flexible, solid-state supercapacitors based on $Ti_3C_2T_x$ films. **a** Schematic illustration of a flexible solid-state supercapacitor based on spin coating $Ti_3C_2T_x$ MXene on polyethylene terephthalate (PET) sheets as electrodes and solid ionogel as the electrolyte. **b** CV curves at various scan rates and **c** galvanostatic charge/discharge (GCD) curves at different current densities for the flexible solid-state device. **d** The volumetric capacitances obtained from GCD and CV. **e** Long-term charge–discharge cycling performance and Coulombic efficiency of the $Ti_3C_2T_x$-based flexible solid-state device. Inset in (**e**): the typical GCD curves upon cycling. **f** CV curves of the $Ti_3C_2T_x$ device bent to different angles at 50 mV s^{-1}. Inset in (**f**): optical image of the transparent flexible ultra-thin supercapacitor [with permission Ref. [81] 2017 (open access) Royal Society of Chemistry (RSC)]

5.4 MXenes for Batteries

The exploitation of fossil fuel reservoirs due to the expanded energy usage has forced researchers to develop alternate energy generation technologies, such as solar, water, and wind. Although the aforementioned promising renewable technologies remarkably contribute toward energy production; however, they are geographically intermittent. Thus, the urgency of the energy storage devices was realized, which can efficiently function and power the required gadgets irrespective of the geography and surrounding atmosphere. When discussing energy storage devices, batteries, especially lithium batteries, have demonstrated superior electrochemical performance over other alternatives. Despite the supremacy of lithium batteries, they suffer from low natural abundance and safety aspects due to the hazardous undesirable Li-dendrite formation. Thus, limiting their usage in high-energy density lithium metal batteries. Therefore, the alternatives with huge profuse in earth's crust, such as monovalent, sodium (Na), potassium (K) batteries, and multivalent, magnesium (Mg), calcium (Ca), zinc (Zn), aluminum (Al) batteries, etc., required to be extensively explored to cope with the pressing global demand.

In the above context, advanced material design is essential, which can store the corresponding charged species, such as Li^+, Na^+, K^+, Mg^{2+}, Ca^{2+}, Zn^{2+}, and Al^{3+},

within its structure for respective metal-ion batteries. Graphite, carbonaceous, and 2D layered materials have been of great interest that are capable of reversibly storing specific metal ions. For instance, graphite and its derivatives (graphene oxide, reduced graphene oxide, graphene) are suitable for Li and K-ion batteries; however, they cannot intercalate Na-ions due to specific layer spacing and higher activation energy. Similarly, hard carbon is ideal for Na-ion batteries compared to the alternatives. Therefore, significant efforts were devoted toward extensive research innovation to develop a new class of 2D materials capable of intercalating the above-mentioned ions for respective metal-ion batteries. Eventually, perseverance was attained in the last decade by introducing a family of different 2D layered structured materials like MXenes. The structure of the MXene phase can be tuned during the transformation step of the etching of the MAX phase, which plays a vital role in its application type. For example, smaller interlayer spacing suffices for intercalating smaller ions, i.e., Al^{3+}, Li^{+}, Mg^{2+}, Zn^{2+}, etc., for respective metal-ion batteries; in contrast, larger ions, i.e., Na^{+}, K^{+}, Ca^{2+}, etc. demand a larger interlayer spacing. Therefore, the same MXene is not employable for each kind of metal-ion battery, which necessitates the interlayer-cum-structure tuning of MXenes for applicability in distinct metal-ion batteries due to their inherently intercalating demand. The MXene's ($M_{n+1}X_nT_x$) structure can be tuned by introducing a combination of suitable early transition metal (M = Ti, V, Sc, Mo, etc.), carbon or nitrogen (X), the functional groups (T_x = O, F, OH, Cl, etc.), and the process adopted, where M and X support the 2D skeleton, and n and functional groups participate in tuning the interlayer spacing. The process depends on structural and/or layer spacing modification of MXenes for battery application, which is described in details in references [82–84].

In the above structural and morphological context of MXenes, Greaves et al. [85] have summarized the various shapes of MXenes, which can be transformed into crumpled flocs, delaminated sheets, hollow spheres, nanoribbons, nanopillars, and composites, according to the required applications for different metal-ion batteries. Moreover, Ming et al. [84] have discussed the individual usage of modified MXenes via structural engineering, regulating interlayer spacing, substitution, and surface modification, forming their derivatives, and making hybrid composites for employing them in suitable battery applications, such as single/alkali-ion batteries (i.e., Li^{+}, Na^{+}, K^{+}, etc.), multivalent-ion batteries (i.e., Al^{3+}, Mg^{2+}, Zn^{2+}, etc.), and metal batteries. The flexibility of interlayer tuning via employing different synthesis routes facilitates suitable ionic diffusion within its layered structure sans structural deterioration, resulting in superior rate performance and better electrochemical cyclic stability. The previously mentioned manipulatable property of MXenes makes them more suitable electrodes, especially intercalation-type, than commercially used graphite or other 2D carbon materials for metal batteries. Another major difference between graphite and MXene is their ion-storing potential. In graphite, the lithium-ion gets intercalated close to 0.1 V versus Li/Li^{+}, which is vulnerable to Li-plating, raising serious safety concerns. Whereas MXenes store lithium ions at around 0.5 V versus Li/Li^{+}, avoiding the possibility of lithium plating, thus, eliminating the safety risks. Therefore, employing MXenes instead of graphite in lithium batteries improves the safety

aspects; however, the cell voltage gets sacrificed due to the higher storing potential of MXenes.

Electronic properties of electrode materials are also a key requirement or beneficial factor and play a critical role in enhancing the electrochemical performance of energy storage devices. In addition to higher ionic diffusion, MXenes exhibit excellent electronic conductivity similar to its competitor graphene due to the available pool of electrons. Researchers have revealed that most of the MXenes have metal-like electronic properties; however, they can be significantly tuned by surface terminations or surface functional groups [86]. For example, $Ti_3C_2(OH)_2$, i.e., OH functional group, exhibits a narrow band gap of 0.05 eV, whereas $Ti_3C_2F_2$, i.e., F functional group, exhibits a wide band gap of 0.1 eV [87]. Not only the surface terminations but orbital hybridization of functional groups, viz., *p* orbitals and transitions metals' *d* orbital could lead MXenes toward semiconductor behavior from metallic behavior. Moreover, the transition metal *M* in MXenes is crucial in delivering the necessary electronic conductivity. For instance, substituting Ti with Mo in titanium carbide-based MXenes transforms the metallic behavior into semiconducting behavior. Therefore, the surface functional groups and their hybridization, transition metals, and their arrangements could vastly alter the electronic conductivity and related properties. The superior electronic conductivity was attributed to the highly aligned coplanar arrangement of MXene flakes/layers possessing metallic free-electron density. The higher electronic conductivity of MXenes facilitates swift electron transport and charge transfer within the electrodes and provides good electrical connectivity, resulting in improved electrochemical performance, proving to be a potential electrodes for electrochemical energy storage devices, i.e., batteries.

As per the above discussion regarding the suitability of MXenes in batteries, major research focuses on employing MXenes via compositing with active anodes due to the possibility of self-discharge from MXenes' layers having larger interlayer spacing. In this regard, synthesized MXene-anode composites are used in monovalent lithium-ion and sodium-ion batteries, as shown in Fig. 5.14 [88, 89]. Figure 5.14a reveals the SEM image of the as-prepared $Li_4Ti_5O_{12}$-MXene ($Ti_3C_2T_x$) composite, revealing a clear laminated 2D layered flake-shaped morphology corresponding to $Ti_3C_2T_x$ MXene structure. $Li_4Ti_5O_{12}$ has nucleated from the defect sites in the MXene, which can be observed on the sides of the MXene layers. Such composite morphology was attained by etching the MAX (Ti_3AlC_2) phase with HF resulting in MXene ($Ti_3C_2T_x$), followed by treating MXene with LiOH in the presence of H_2O_2 to obtain $Li_4Ti_5O_{12}$-MXene composite. A similar synthesis process was adopted by Huang et al. [89] to achieve sandwich-type $Na_{0.23}TiO_2$-MXene (Ti_3C_2) composite by treating Ti_3C_2 MXene with NaOH and oxidant. The sandwich-type composite morphology is shown in Fig. 5.14b. The synthesized MXene composites were tested in lithium-ion half cells to evaluate their performance. Figure 5.14c shows the cyclic voltammogram (CV) of $Li_4Ti_5O_{12}$-MXene composite against pristine lithium in a half cell at various scan rates viz., 0.2, 0.4, 0.8, 1, and 2 mV s^{-1}. The CV curves demonstrate an excellent rate capability due to negligible distortion of the CV profiles on varying the scan rate. The superior rate performance corresponds to the unique morphological features and the presence of MXene. The $Li_4Ti_5O_{12}$ particles are grown on the surface of MXene,

thus, directly attached to them, and MXene is directly in contact with the electrolyte, allowing easy facilitation of Li-ions from the electrolyte to MXene and $Li_4Ti_5O_{12}$ particles. Whereas MXene also facilitates fast electron conduction, resulting in an interconnected path of electrons throughout the structure, enhancing the reaction rate during intercalation/de-intercalation of Li-ions. Therefore, $Li_4Ti_5O_{12}$-Mxene composite exhibits both fast Li-ion diffusion and rapid electronic conduction, proving superior rate performance. Similarly, Fig. 5.14d demonstrates the first three CV cycles of sandwich-type $Na_{0.23}TiO_2$-MXene composite at a scan rate of 1 mV s^{-1}. Except for the first cycle, which includes the formation of solid-electrolyte interphase (SEI), the following cycles overlap with each other, revealing good reversibility. The long galvanostatic cycling of $Li_4Ti_5O_{12}$-Mxene composite was evaluated, as shown in Fig. 5.14e, which revealed a discharge capacity of 178 mAh g^{-1} after 500 cycles at a high current density of 5 A g^{-1} with maintaining the Coulombic efficiency of nearly 100%. This excellent electrochemical cycling stability was assigned to the structural stability, unique morphology, minimal volume expansion, and rapid ionic and electronic diffusion/conduction. The gradual rise in reversible capacity over the cycling is due to the widening of the MXenes' interlayer spacing via trapping Li-ions and infiltration of non-coordinated solvent species. A similar observation was made for sandwich-type $Na_{0.23}TiO_2$-MXene composite at the same current density of 5 A g^{-1}, as shown in Fig. 5.14f. Furthermore, sandwich-type $Na_{0.23}TiO_2$-MXene composite was subjected to galvanostatic cycling against sodium (in a sodium-ion half cell), as shown in Fig. 5.14g. The remarkable cyclic stability was attributed to the above explanation. However, the size of Na-ion is larger than the Li-ions, the expanded MXenes having more interlayer spacing can explain Na-ion storage, which can successfully intercalate/de-intercalate larger Na-ions. Therefore, MXenes or MXene-based composites can easily store monovalent or alkali metal ions for alkali metal(ion) batteries with superior electrochemical performance.

MXenes have demonstrated the capability of storing monovalent alkali-ions and possess the potential to intercalate multivalent ions, such as Al^{3+}, Mg^{2+}, Zn^{2+}, etc., for respective metal-ion batteries. For instance, Xu et al. [90] revealed the storage of Mg^{2+} ions by Ti_3C_2 MXene via pre-storing a cationic surfactant (CTAB). Along with the experimental shreds of evidence, theoretical simulations also verified that the Mg-ion diffusion barrier could be reduced by intercalating CTA^+ cations. Therefore, Mg-ions intercalation/de-intercalation between MXene layers gets significantly improved, resulting in the volumetric capacity of 300 mAh cm^{-3} at a current density of 50 mA g^{-1}. Moreover, Vahid Mohammadi et al. [91] employed MXenes for Al^{3+} storage for high-capacity Al-ion batteries, as presented in Fig. 5.15. Figure 5.15a revealed the typical MXene layered structure of V_2CT_x after etching the corresponding MAX phase (V_2AlC) with concentrated HF for 92 h at room temperature. The galvanostatic potential profile (Fig. 5.15b) indicated a substantial irreversible discharge capacity of about 335 mAh g^{-1} at a current density of 10 mA g^{-1}, which corresponds to chloroaluminate anions' dissolution and SEI formation. Post the first cycle; the second discharge cycle delivered a specific capacity of about 178 mAh g^{-1}, corresponding to $V_2Al_{0.26}CT_x$ intercalated phase. Broad plateaus observed in the potential profile indicated a wide interlayer spacing possessing a range of potential

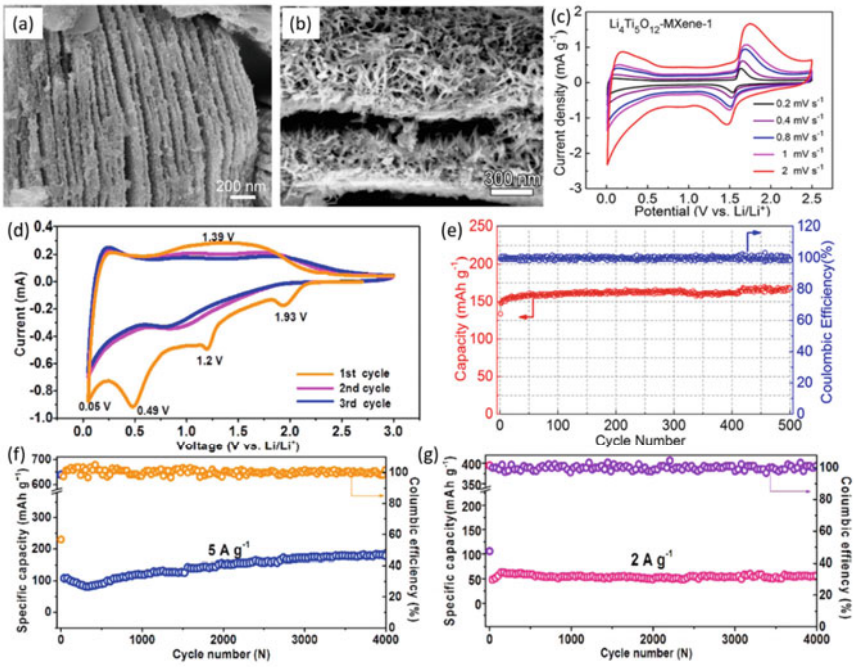

Fig. 5.14 **a** SEM image of $Li_4Ti_5O_{12}$-Mxene ($Ti_3C_2T_x$) composite. **b** SEM image of sandwich-type $Na_{0.23}TiO_2$-MXene (Ti_3C_2) composite. **c** cyclic voltammograms of $Li_4Ti_5O_{12}$-MXene composite at different scan rates, viz., 0.2, 0.4, 0.8, 1, and 2 mV s^{-1} for lithium-ion batteries (LIBs). **d** cyclic voltammograms of sandwich-type $Na_{0.23}TiO_2$-MXene composite at a scan rate of 1 mV s^{-1} for LIBs. **e** galvanostatic cycling of $Li_4Ti_5O_{12}$-MXene composite at a high current density of 5 A g^{-1} for LIBs. **f** galvanostatic cycling of sandwich-type $Na_{0.23}TiO_2$-MXene composite at a high current density of 5 A g^{-1} for LIBs. **g** galvanostatic cycling of sandwich-type $Na_{0.23}TiO_2$-MXene composite at a high current density of 2 A g^{-1} for sodium-ion batteries (SIBs) [with permission from Refs. [88, 89] Copyright 2018 Elsevier]

for intercalation/de-intercalation, which was confirmed with a cyclic voltammogram (as shown in Fig. 5.15c), revealing the corresponding cathodic and anodic peaks. Figure 5.15b clearly shows that there is a severe capacity decay over the cycling for multilayer MXene. Therefore, by further treatment, MXene was modified to a few-layer and subjected to electrochemical cycling (Fig. 5.15d, e). By transforming the multilayer MXene into few-layer MXene, the rapid capacity decay was suppressed; however, a gradual decay was observed, retaining a reversible capacity of 90 mAh g^{-1} after 100 cycles at a higher current density of 100 mA g^{-1}. To evaluate the fast-charging performance of few-layer MXene, a different protocol was employed with a high charge current density of 1000 mA g^{-1} and a low discharge current density of 100 mA g^{-1}. Even at this high charging rate, few-layer MXene was able to retain a specific capacity of 76 mAh g^{-1} after 100 revolutions (Fig. 5.15e). Therefore, the applicability of MXenes is not only limited to alkali metal batteries but

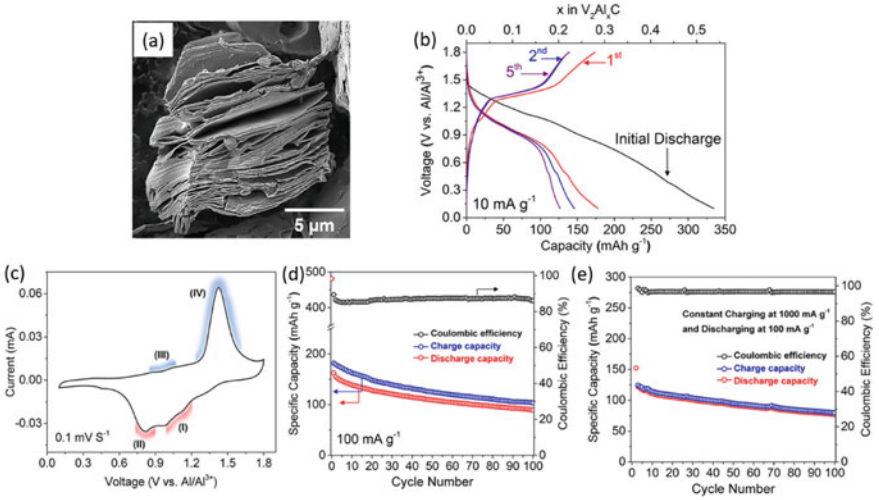

Fig. 5.15 **a** SEM image of MXene (V_2CT_x), obtained by treating V_2AlC MAX phase with 50% HF for 92 h at room temperature. **b** initial galvanostatic potential profiles of multilayer V_2CT_x MXene electrode against Al-metal anode at a current density of 10 mA g^{-1}. **c** cyclic voltammogram of multilayer V_2CT_x MXene electrode at a scan rate of 0.1 mV s^{-1} in a potential window of 0.1–1.8 V (V vs. Al/Al^{3+}). **d** galvanostatic cycling of few-layer V_2CT_x MXene electrode at a current density of 100 mA g^{-1}. **e** galvanostatic cycling of few-layer V_2CT_x MXene electrode at a charge current density of 1000 mA g^{-1} and discharge current density of 100 mA g^{-1}, showing fast-charging capability [with permission from Ref. [91] Copyright 2017 American Chemical Society]

also multivalent-ion batteries, metal-sulfur batteries, and metal batteries. However, the research progress on multivalent-ion batteries, metal-sulfur batteries, and metal batteries is limited. According to the current research progress, structure modification, interlayer spacing tuning, surface or functional group substitution, transition metal doping, and choice of synthesis process are a few strategies to enhance the properties of MXenes for an improvement in electrochemical performance for various metal(ion) battery applications.

5.5 Conclusion

The material composition and architecture of MXenes widen the scope of their utilization in energy conversion and storage devices. Their performance improvement procedure (energy and power density) depends on the surface features. The edge sites and the electronic band structure of MXenes enhance their water-splitting performance to replace precious metal (noble metal) electrocatalysts in water electrolyzer systems. The vertically aligned nanosheets of MXenes decrease the diffusion resistance to enhance the supercapacitor performance. Moreover, the reversible intercalation of various electrolyte ions in the expanded layers of MXenes makes

them potential candidates for new-generation supercapacitors. The terminated functional groups on the MXenes play an essential role in energy storage regarding ion adsorption and ion diffusion barriers. With the good qualities of flexible morphologies, wide and tunable interlayer spacing, superior ionic diffusivity, higher electronic conductivity, and reversible volume expansion, MXenes are capable of intercalating/de-intercalate alkali-ions and multivalent ions due to their inherent large interlayer spacing. The surface groups on the MXenes control the in-situ growth of active species responsible for decreasing the charge–discharge process.

Despite the extensive efforts of researchers and promising qualities with excellent electrochemical performance in supercapacitors and batteries, certain issues are still prevailing in commercializing the MXenes, such as

1. Understanding the intercalation mechanism of multivalent ions. One has to explore the relationship between the interlayer spacing and diffusion barrier.
2. Requirement of facile and innovative synthesis strategies and etching methods. For instance, mostly HF is employed in etching the MAX phase to obtain MXenes, which is unsafe and harmful for humans and the environment.
3. To explore the doping and defect engineering of MXene electrocatalyst for water-splitting application. The potential doping (metal species) as redox sites in energy storage systems is yet to be explored. The theoretical and experimental results may provide a breakthrough energy and power density of MXene-based energy conversion and storage devices.

References

1. L. Huo, B. Liu, G. Zhang, J. Zhang, Universal strategy to fabricate a two-dimensional layered mesoporous Mo_2C electrocatalyst hybridized on graphene sheets with high activity and durability for hydrogen generation. ACS Appl. Mater. Interfaces **8**, 18107–18118 (2016). https://doi.org/10.1021/acsami.6b05007
2. H. Tao, Q. Fan, T. Ma, S. Liu, H. Gysling, J. Texter et al., Two-dimensional materials for energy conversion and storage. Prog. Mater. Sci. **111**, 100637 (2020). https://doi.org/10.1016/j.pmatsci.2020.100637
3. M. Naguib, J. Halim, J. Lu, K.M. Cook, L. Hultman, Y. Gogotsi et al., New twodimensional niobium and vanadium carbides as promising materials for Liion batteries partners 1–2 (2016). https://doi.org/10.1021/ja405735d
4. Y. Wang, T. Guo, Z. Tian, K. Bibi, Y.Z. Zhang, H.N. Alshareef, MXenes for energy harvesting. Adv. Mater. **34**, 1–22 (2022). https://doi.org/10.1002/adma.202108560
5. J. Li, F. Zeng, J.K. El-Demellawi, Q. Lin, S. Xi, J. Wu et al., Nb_2CT_xMXene cathode for high-capacity rechargeable aluminum batteries with prolonged cycle lifetime. ACS Appl. Mater. Interfaces **14**, 45254–45262 (2022). https://doi.org/10.1021/acsami.2c09765
6. J. Liu, W. Peng, Y. Li, F. Zhang, X. Fan, 2D MXene-based materials for electrocatalysis. Trans. Tianjin Univ. **26**, 149–171 (2020). https://doi.org/10.1007/s12209-020-00235-x
7. R. Garg, A. Agarwal, M. Agarwal, A review on MXene for energy storage application: effect of interlayer distance. Mater. Res. Express **7** (2020). https://doi.org/10.1088/2053-1591/ab750d
8. R.M. Ronchi, J.T. Arantes, S.F. Santos, Synthesis, structure, properties and applications of MXenes: current status and perspectives. Ceram. Int. **45**, 18167–18188 (2019). https://doi.org/10.1016/j.ceramint.2019.06.114

9. S.T. Mahmud, M.M. Hasan, S. Bain, S.T. Rahman, M. Rhaman, M.M. Hossain et al., Multilayer MXene heterostructures and nanohybrids for multifunctional applications: a review. ACS Mater. Lett. **4**, 1174–1206 (2022). https://doi.org/10.1021/acsmaterialslett.2c00175
10. P. Das, Z.S. Wu, MXene for energy storage: present status and future perspectives. J. Phys. Energy **2** (2020). https://doi.org/10.1088/2515-7655/ab9b1d
11. F.R. Fan, W. Wu, Emerging devices based on two-dimensional monolayer materials for energy harvesting. Research **2019**, 1–16 (2019). https://doi.org/10.34133/2019/7367828
12. Z. Fu, N. Wang, D. Legut, C. Si, Q. Zhang, S. Du et al., Rational design of flexible two-dimensional MXenes with multiple functionalities. Chem. Rev. **119**, 11980–12031 (2019). https://doi.org/10.1021/acs.chemrev.9b00348
13. J. Song, C. Wei, Z.F. Huang, C. Liu, L. Zeng, X. Wang et al., A review on fundamentals for designing oxygen evolution electrocatalysts. Chem. Soc. Rev. **49**, 2196–2214 (2020). https://doi.org/10.1039/c9cs00607a
14. R. Ahmad, S. Upadhyay, O.P. Pandey, A review on recent advances and progress in Mo_2C@C: a suitable and stable electrocatalyst for HER. Int. J. Hydrog. Energy (2022). https://doi.org/10.1016/j.ijhydene.2022.12.179
15. S. Wang, A. Lu, C.J. Zhong, Hydrogen production from water electrolysis: role of catalysts. Nano Converge **8** (2021). https://doi.org/10.1186/s40580-021-00254-x
16. N. Yuan, Q. Jiang, J. Li, J. Tang, A review on non-noble metal based electrocatalysis for the oxygen evolution reaction. Arab. J. Chem. **13**, 4294–4309 (2020). https://doi.org/10.1016/j.arabjc.2019.08.006
17. S.M. Ibn Shamsah, Earth-abundant electrocatalysts for water splitting: current and future directions. Catalysts **11** (2021). https://doi.org/10.3390/catal11040429
18. H. Yuan, L. Kong, T. Li, Q. Zhang, A review of transition metal chalcogenide/graphene nanocomposites for energy storage and conversion. Chin. Chem. Lett. **28**, 2180–2194 (2017). https://doi.org/10.1016/j.cclet.2017.11.038
19. Y.C. Kimmel, X. Xu, W. Yu, X. Yang, J.G. Chen, Trends in electrochemical stability of transition metal carbides and their potential use as supports for low-cost electrocatalysts. ACS Catal. **4**, 1558–1562 (2014). https://doi.org/10.1021/cs500182h
20. D.J. Ham, J.S. Lee, Transition metal carbides and nitrides as electrode materials for low temperature fuel cells. Energies **2**, 873–899 (2009). https://doi.org/10.3390/en20400873
21. H. Yan, Y. Xie, Y. Jiao, A. Wu, C. Tian, X. Zhang et al., Holey reduced graphene oxide coupled with an Mo_2N–Mo_2C heterojunction for efficient hydrogen evolution. Adv. Mater. **30** (2018). https://doi.org/10.1002/adma.201704156
22. R.B. Levy, M. Boudart, Platinum-like behavior of tungsten carbide in surface catalysis. Science **181**(80), 547–549 (1973)
23. J.S. Lee, S.T. Oyama, M. Boudart, Molybdenum carbide catalysts. J. Catal. **106**, 125–133 (1987). https://doi.org/10.1016/0021-9517(87)90218-1
24. M. Naguib, O. Mashtalir, J. Carle, V. Presser, J. Lu, L. Hultman et al., Two-dimensional transition metal carbides. ACS Nano **6**, 1322–1331 (2012). https://doi.org/10.1021/nn204153h
25. J. Liu, T. Chen, P. Juan, W. Peng, Y. Li, F. Zhang et al., Hierarchical cobalt borate/MXenes hybrid with extraordinary electrocatalytic performance in oxygen evolution reaction. Chemsuschem **11**, 3758–3765 (2018). https://doi.org/10.1002/cssc.201802098
26. Z. Kang, M.A. Khan, Y. Gong, R. Javed, Y. Xu, D. Ye et al., Recent progress of MXenes and MXene-based nanomaterials for the electrocatalytic hydrogen evolution reaction. J. Mater. Chem. A **9**, 6089–6108 (2021). https://doi.org/10.1039/d0ta11735h
27. K.R.G. Lim, A.D. Handoko, L.R. Johnson, X. Meng, M. Lin, G.S. Subramanian et al., 2H-MoS_2on Mo_2CT_xMXene nanohybrid for efficient and durable electrocatalytic hydrogen evolution. ACS Nano **14**, 16140–16155 (2020). https://doi.org/10.1021/acsnano.0c08671
28. B.C. Wyatt, A. Thakur, K. Nykiel, Z.D. Hood, S.P. Adhikari, K.K. Pulley et al., Design of atomic ordering in $Mo_2Nb_2C_3T_x$ MXenes for hydrogen evolution electrocatalysis. Nano Lett. (2023). https://doi.org/10.1021/acs.nanolett.2c04287
29. J. Abed, S. Ahmadi, L. Laverdure, A. Abdellah, C.P. O'Brien, K. Cole et al., In situ formation of nano Ni–Co oxyhydroxide enables water oxidation electrocatalysts durable at high current densities. Adv. Mater. **33** (2021). https://doi.org/10.1002/adma.202103812

30. M.P. Browne, D. Tyndall, V. Nicolosi, The potential of MXene materials as a component in the catalyst layer for the oxygen evolution reaction. Curr. Opin. Electrochem. **34**, 101021 (2022). https://doi.org/10.1016/j.coelec.2022.101021
31. C.F. Du, X. Sun, H. Yu, W. Fang, Y. Jing, Y. Wang et al., $V_4C_3T_x$ MXene: a promising active substrate for reactive surface modification and the enhanced electrocatalytic oxygen evolution activity. InfoMat **2**, 950–959 (2020). https://doi.org/10.1002/inf2.12078
32. Z.W. Seh, K.D. Fredrickson, B. Anasori, J. Kibsgaard, A.L. Strickler, M.R. Lukatskaya et al., Two-dimensional molybdenum carbide (MXene) as an efficient electrocatalyst for hydrogen evolution. ACS Energy Lett. **1**, 589–594 (2016). https://doi.org/10.1021/acsenergylett.6b00247
33. A.D. Handoko, K.D. Fredrickson, B. Anasori, K.W. Convey, L.R. Johnson, Y. Gogotsi et al., Tuning the basal plane functionalization of two-dimensional metal carbides (MXenes) to control hydrogen evolution activity. ACS Appl. Energy Mater. **1**, 173–180 (2018). https://doi.org/10.1021/acsaem.7b00054
34. S. Li, P. Tuo, J. Xie, X. Zhang, J. Xu, J. Bao et al., Ultrathin MXene nanosheets with rich fluorine termination groups realizing efficient electrocatalytic hydrogen evolution. Nano Energy **47**, 512–518 (2018). https://doi.org/10.1016/j.nanoen.2018.03.022
35. Y. Jiang, T. Sun, X. Xie, W. Jiang, J. Li, B. Tian et al., Oxygen-functionalized ultrathin $Ti_3C_2T_x$ MXene for enhanced electrocatalytic hydrogen evolution. Chemsuschem **12**, 1368–1373 (2019). https://doi.org/10.1002/cssc.201803032
36. M.H. Tran, T. Schäfer, A. Shahraei, M. Dürrschnabel, L. Molina-Luna, U.I. Kramm et al., Adding a new member to the MXene family: synthesis, structure, and electrocatalytic activity for the hydrogen evolution reaction of $V_4C_3T_x$. ACS Appl. Energy Mater. **1**, 3908–3914 (2018). https://doi.org/10.1021/acsaem.8b00652
37. Y. Yoon, A.P. Tiwari, M. Lee, M. Choi, W. Song, J. Im et al., Enhanced electrocatalytic activity by chemical nitridation of two-dimensional titanium carbide MXene for hydrogen evolution. J. Mater. Chem. A **6**, 20869–20877 (2018). https://doi.org/10.1039/C8TA08197B
38. W. Yuan, L. Cheng, Y. An, H. Wu, N. Yao, X. Fan et al., MXene nanofibers as highly active catalysts for hydrogen evolution reaction. ACS Sustain. Chem. Eng. **6**, 8976–8982 (2018). https://doi.org/10.1021/acssuschemeng.8b01348
39. C.F. Du, X. Sun, H. Yu, Q. Liang, K.N. Dinh, Y. Zheng et al., Synergy of Nb doping and surface alloy enhanced on water-Alkali electrocatalytic hydrogen generation performance in Ti-based MXene. Adv. Sci. **6**, 1–7 (2019). https://doi.org/10.1002/advs.201900116
40. Z. Li, Z. Qi, S. Wang, T. Ma, L. Zhou, Z. Wu et al., In situ formed Pt_3Ti nanoparticles on a two-dimensional transition metal carbide (MXene) used as efficient catalysts for hydrogen evolution reactions. Nano Lett. **19**, 5102–5108 (2019). https://doi.org/10.1021/acs.nanolett.9b01381
41. Y. Yuan, H. Li, L. Wang, L. Zhang, D. Shi, Y. Hong et al., Achieving highly efficient catalysts for hydrogen evolution reaction by electronic state modification of platinum on versatile $Ti_3C_2T_x$ (MXene). ACS Sustain. Chem. Eng. **7**, 4266–4273 (2019). https://doi.org/10.1021/acssuschemeng.8b06045
42. S.Y. Pang, Y.T. Wong, S. Yuan, Y. Liu, M.K. Tsang, Z. Yang et al., Universal strategy for HF-free facile and rapid synthesis of two-dimensional MXenes as multifunctional energy materials. J. Am. Chem. Soc. **141**, 9610–9616 (2019). https://doi.org/10.1021/jacs.9b02578
43. J. Liang, C. Ding, J. Liu, T. Chen, W. Peng, Y. Li et al., Heterostructure engineering of Co-doped MoS_2 coupled with Mo_2CT_X MXene for enhanced hydrogen evolution in alkaline media. Nanoscale **11**, 10992–11000 (2019). https://doi.org/10.1039/c9nr02085c
44. J. Filip, S. Zavahir, L. Lorencova, T. Bertok, A.B. Yousaf, K.A. Mahmoud et al. Tailoring electrocatalytic properties of Pt nanoparticles grown on $Ti_3C_2T_X$ MXene surface. J. Electrochem. Soc. **166**, H54–H62 (2019). https://doi.org/10.1149/2.0991902jes
45. N.H. Attanayake, S.C. Abeyweera, A.C. Thenuwara, B. Anasori, Y. Gogotsi, Y. Sun et al., Vertically aligned MoS_2 on Ti_3C_2 (MXene) as an improved HER catalyst. J. Mater. Chem. A **6**, 16882–16889 (2018). https://doi.org/10.1039/c8ta05033c
46. B. Cui, B. Hu, J. Liu, M. Wang, Y. Song, K. Tian et al., Solution-plasma-assisted bimetallic oxide alloy nanoparticles of Pt and Pd embedded within two-dimensional $Ti_3C_2T_x$ nanosheets

as highly active electrocatalysts for overall water splitting. ACS Appl. Mater. Interfaces **10**, 23858–23873 (2018). https://doi.org/10.1021/acsami.8b06568
47. C.F. Du, K.N. Dinh, Q. Liang, Y. Zheng, Y. Luo, J. Zhang et al., Self-assemble and in situ formation of $Ni_{1-x}Fe_xPS_3$ nanomosaic-decorated MXene hybrids for overall water splitting. Adv. Energy Mater. **8**, 1–9 (2018). https://doi.org/10.1002/aenm.201801127
48. J. Liu, Y. Liu, D. Xu, Y. Zhu, W. Peng, Y. Li et al., Hierarchical "nanoroll" like $MoS_2/Ti_3C_2T_x$ hybrid with high electrocatalytic hydrogen evolution activity. Appl. Catal. B Environ. **241**, 89–94 (2019). https://doi.org/10.1016/j.apcatb.2018.08.083
49. L. Xiu, Z. Wang, M. Yu, X. Wu, J. Qiu, Aggregation-resistant 3D MXene-based architecture as efficient bifunctional electrocatalyst for overall water splitting. ACS Nano **12**, 8017–8028 (2018). https://doi.org/10.1021/acsnano.8b02849
50. M. Yu, S. Zhou, Z. Wang, J. Zhao, J. Qiu, Boosting electrocatalytic oxygen evolution by synergistically coupling layered double hydroxide with MXene. Nano Energy **44**, 181–190 (2018). https://doi.org/10.1016/j.nanoen.2017.12.003
51. L. Zhao, B. Dong, S. Li, L. Zhou, L. Lai, Z. Wang et al., Interdiffusion reaction-assisted hybridization of two-dimensional metal-organic frameworks and $Ti_3C_2T_x$ nanosheets for electrocatalytic oxygen evolution. ACS Nano **11**, 5800–5807 (2017). https://doi.org/10.1021/acsnano.7b01409
52. T.Y. Ma, J.L. Cao, M. Jaroniec, S.Z. Qiao, Interacting carbon nitride and titanium carbide nanosheets for high-performance oxygen evolution. Angew. Chem. Int. Ed. **55**, 1138–1142 (2016). https://doi.org/10.1002/anie.201509758
53. Y. Tang, C. Yang, Y. Yang, X. Yin, W. Que, J. Zhu, Three dimensional hierarchical network structure of S-$NiFe_2O_4$ modified few-layer titanium carbides (MXene) flakes on nickel foam as a high efficient electrocatalyst for oxygen evolution. Electrochim. Acta **296**, 762–770 (2019). https://doi.org/10.1016/j.electacta.2018.11.083
54. H. Zou, B. He, P. Kuang, J. Yu, K. Fan, Metal-organic framework-derived nickel-cobalt sulfide on ultrathin MXene nanosheets for electrocatalytic oxygen evolution. ACS Appl. Mater. Interfaces **10**, 22311–22319 (2018). https://doi.org/10.1021/acsami.8b06272
55. Y. Zhang, H. Jiang, Y. Lin, H. Liu, Q. He, C. Wu et al., In situ growth of cobalt nanoparticles encapsulated nitrogen-doped carbon nanotubes among $Ti_3C_2T_x$ (MXene) matrix for oxygen reduction and evolution. Adv. Mater. Interfaces **5**, 1–9 (2018). https://doi.org/10.1002/admi.201800392
56. T. Brousse, D. Bélanger, J.W. Long, To be or not to be pseudocapacitive? J. Electrochem. Soc. **162**, A5185–A5189 (2015). https://doi.org/10.1149/2.0201505jes
57. M.R. Lukatskaya, S. Kota, Z. Lin, M.Q. Zhao, N. Shpigel, M.D. Levi et al., Ultra-high-rate pseudocapacitive energy storage in two-dimensional transition metal carbides. Nat. Energy **6**, 1–6 (2017). https://doi.org/10.1038/nenergy.2017.105
58. A. Sharma, P. Mane, B. Chakraborty, C.S. Rout, 1T-VS2/MXene hybrid as a superior electrode material for asymmetric supercapacitors: experimental and theoretical investigations. ACS Appl. Energy Mater. **4**, 14198–14209 (2021). https://doi.org/10.1021/acsaem.1c02959
59. Z.S. Iroc, C. Subramani, S.S. Dash, A brief review on electrode materials for supercapacitor **11**, 10628–10643 (2016). https://doi.org/10.20964/2016.12.50
60. J.R. Miller, Engineering electrochemical capacitor applications. J. Power. Sources **326**, 726–735 (2016). https://doi.org/10.1016/j.jpowsour.2016.04.020
61. S.A. Thomas, J. Cherusseri, A review of Nb_2CT_x MXene as an emerging 2D material: synthesis, applications in rechargeable batteries and supercapacitors, progress, and outlook. Energy Fuels (2023). https://doi.org/10.1021/acs.energyfuels.3c00503
62. M. He, K. Fic, E. Frackowiak, P. Novák, E.J. Berg, Ageing phenomena in high-voltage aqueous supercapacitors investigated by in situ gas analysis. Energy Environ. Sci. **9**, 623–633 (2016). https://doi.org/10.1039/c5ee02875b
63. C. Wang, X. Wang, L. Zhang, L. Yin, MXene for high energy and power density: a perspective. J. Phys. Energy **2** (2020). https://doi.org/10.1088/2515-7655/abab66
64. J. Luo, W. Zhang, H. Yuan, C. Jin, L. Zhang, H. Huang et al., Pillared structure design of MXene with ultralarge interlayer spacing for high-performance lithium-ion capacitors. ACS Nano **11**, 2459–2469 (2017). https://doi.org/10.1021/acsnano.6b07668

65. H. He, J. Wang, Q. Xia, L. Wang, Q. Hu, A. Zhou, Effect of electrolyte on supercapacitor performance of two-dimensional molybdenum carbide (Mo_2CT_x) MXene prepared by hydrothermal etching. Appl. Surf. Sci. 568 (2021). https://doi.org/10.1016/j.apsusc.2021.150971
66. Q. Zhu, J. Li, P. Simon, B. Xu, Two-dimensional MXenes for electrochemical capacitor applications: progress, challenges and perspectives. Energy Storage Mater. **35**, 630–660 (2021). https://doi.org/10.1016/j.ensm.2020.11.035
67. Y. Gogotsi, B. Anasori, The rise of MXenes. ACS Nano **13**, 8491–8494 (2019). https://doi.org/10.1021/acsnano.9b06394
68. M. Hu, T. Hu, Z. Li, Y. Yang, R. Cheng, J. Yang et al., Surface functional groups and interlayer water determine the electrochemical capacitance of $Ti_3C_2T_x$ MXene. ACS Nano **12**, 3578–3586 (2018). https://doi.org/10.1021/acsnano.8b00676
69. Y. Xie, M. Naguib, V.N. Mochalin, M.W. Barsoum, Y. Gogotsi, X. Yu et al., Role of surface structure on li-ion energy storage capacity of two-dimensional transition-metal carbides. J. Am. Chem. Soc. **136**, 6385–6394 (2014). https://doi.org/10.1021/ja501520b
70. K. Maleski, V.N. Mochalin, Y. Gogotsi, Dispersions of two-dimensional titanium carbide MXene in organic solvents. Chem. Mater. **29**, 1632–1640 (2017). https://doi.org/10.1021/acs.chemmater.6b04830
71. M.R. Lukatskaya, O. Mashtalir, C.E. Ren, Y. Dall'Agnese, P. Rozier, P.L. Taberna et al. Cation intercalation and high volumetric capacitance of two-dimensional titanium carbide. Science **341**(80), 1502–1505 (2013). https://doi.org/10.1126/science.1241488
72. M. Naguib, V.N. Mochalin, M.W. Barsoum, Y. Gogotsi, 25th anniversary article: MXenes: a new family of two-dimensional materials. Adv. Mater. **26**, 992–1005 (2014). https://doi.org/10.1002/adma.201304138
73. J. Pang, R.G. Mendes, A. Bachmatiuk, L. Zhao, H.Q. Ta, T. Gemming et al., Applications of 2D MXenes in energy conversion and storage systems. Chem. Soc. Rev. **48**, 72–133 (2019). https://doi.org/10.1039/c8cs00324f
74. Y. Sun, Q. Wu, Y. Xu, H. Bai, C. Li, G. Shi, Highly conductive and flexible mesoporous graphitic films prepared by graphitizing the composites of graphene oxide and nanodiamond. J. Mater. Chem. **21**, 7154–7160 (2011). https://doi.org/10.1039/c0jm04434b
75. A. Burke, R&D considerations for the performance and application of electrochemical capacitors. Electrochim. Acta **53**, 1083–1091 (2007). https://doi.org/10.1016/j.electacta.2007.01.011
76. D. Pech, M. Brunet, H. Durou, P. Huang, V. Mochalin, Y. Gogotsi et al., Ultrahigh-power micrometre-sized supercapacitors based on onion-like carbon. Nat. Nanotechnol. **5**, 651–654 (2010). https://doi.org/10.1038/nnano.2010.162
77. M. Zhu, Y. Huang, Q. Deng, J. Zhou, Z. Pei, Q. Xue et al., Highly flexible, freestanding supercapacitor electrode with enhanced performance obtained by hybridizing polypyrrole chains with MXene. Adv. Energy Mater. **6** (2016). https://doi.org/10.1002/aenm.201600969
78. Y. Dall'Agnese, M.R. Lukatskaya, K.M Cook, P.L. Taberna, Y. Gogotsi, P. Simon, High capacitance of surface-modified 2D titanium carbide in acidic electrolyte. Electrochem. Commun. **48**, 118–122 (2014). https://doi.org/10.1016/j.elecom.2014.09.002
79. A. Zhang, R. Liu, J. Tian, W. Huang, J. Liu, MXene-based nanocomposites for energy conversion and storage applications. Chem. A Eur. J. **26**, 6342–6359 (2020). https://doi.org/10.1002/chem.202000191
80. M. Pramanik, V. Malgras, J. Lin, S.M. Alshehri, T. Ahamad, J.H. Kim et al., Electrochemical property of mesoporous crystalline iron phosphonate anode in li-ion rechargeable battery. J. Nanosci. Nanotechnol. **16**, 9180–9185 (2016). https://doi.org/10.1166/jnn.2016.12883
81. L. Qin, J. Jiang, Q. Tao, C. Wang, I. Persson, M. Fahlman et al., A flexible semitransparent photovoltaic supercapacitor based on water-processed MXene electrodes. J. Mater. Chem. A **8**, 5467–5475 (2020). https://doi.org/10.1039/d0ta00687d
82. L. Verger, C. Xu, V. Natu, H.M. Cheng, W. Ren, M.W. Barsoum, Overview of the synthesis of MXenes and other ultrathin 2D transition metal carbides and nitrides. Curr. Opin. Solid State Mater. Sci. **23**, 149–163 (2019). https://doi.org/10.1016/j.cossms.2019.02.001

83. S. Liu, Z. Song, X. Jin, R. Mao, T. Zhang, F. Hu, MXenes for metal-ion and metal-sulfur batteries: synthesis, properties, and electrochemistry. Mater. Rep. Energy **2**, 100077 (2022). https://doi.org/10.1016/j.matre.2021.100077
84. F. Ming, H. Liang, G. Huang, Z. Bayhan, H.N. Alshareef, MXenes for rechargeable batteries beyond the lithium-ion. Adv. Mater. **33**, 1–35 (2021). https://doi.org/10.1002/adma.202004039
85. M. Greaves, S. Barg, M.A. Bissett, MXene-based anodes for metal-ion batteries. Batter Supercaps **3**, 214–235 (2020). https://doi.org/10.1002/batt.201900165
86. Q. Tang, Z. Zhou, P. Shen, Are MXenes promising anode materials for Li ion batteries? Computational studies on electronic properties and Li storage capability of Ti_3C_2 and $Ti_3C_2X_2$ (X = F, OH) monolayer. J. Am. Chem. Soc. **134**, 16909–16916 (2012). https://doi.org/10.1021/ja308463r
87. M. Naguib, M. Kurtoglu, V. Presser, J. Lu, J. Niu, M. Heon et al., Two-dimensional nanocrystals produced by exfoliation of Ti_3AlC_2. Adv. Mater. **23**, 4248–4253 (2011). https://doi.org/10.1002/adma.201102306
88. J. Wang, S. Dong, H. Li, Z. Chen, S. Jiang, L. Wu et al., Facile synthesis of layered $Li_4Ti_5O_{12}$-Ti_3C_2Tx (MXene) composite for high-performance lithium ion battery. J. Electroanal. Chem. **810**, 27–33 (2018). https://doi.org/10.1016/j.jelechem.2017.12.079
89. J. Huang, R. Meng, L. Zu, Z. Wang, N. Feng, Z. Yang et al., Sandwich-like $Na_{0.23}TiO_2$ nanobelt/Ti_3C_2 MXene composites from a scalable in situ transformation reaction for long-life high-rate lithium/sodium-ion batteries. Nano Energy **46**, 20–28 (2018). https://doi.org/10.1016/j.nanoen.2018.01.030
90. M. Xu, S. Lei, J. Qi, Q. Dou, L. Liu, Y. Lu et al., Opening magnesium storage capability of two-dimensional MXene by intercalation of cationic surfactant. ACS Nano **12**, 3733–3740 (2018). https://doi.org/10.1021/acsnano.8b00959
91. A. Vahidmohammadi, A. Hadjikhani, S. Shahbazmohamadi, M. Beidaghi, Two-dimensional vanadium carbide (MXene) as a high-capacity cathode material for rechargeable aluminum batteries. ACS Nano **11**, 11135–11144 (2017). https://doi.org/10.1021/acsnano.7b05350